ISSN 0965-5441, Petroleum Chemistry, 2021, Vol. 61, No. 3, pp. 388–393. © Pleiades Publishing, Ltd., 2021.
Russian Text © The Author(s), 2021, published in Sovremennye Molekulyarnye Sita. Advanced Molecular Sieves, 2021, Vol. 3, No. 1, pp. 143–148.

Magnetic Materials Based on Layered Double Hydroxides

O. V. Nestroinaya[a], I. G. Ryl'tsova[a], E. A. Tarasenko[a], M. N. Yapryntsev[a], A. A. Solov'eva[a], and O. E. Lebedeva[a,*]

[a] *Belgorod State National Research University, Belgorod, 308015 Russia*
**e-mail: OLebedeva@bsu.edu.ru*

Received October 1, 2020; revised October 26, 2020; accepted November 2, 2020

Abstract—Composite materials that contain tetracationic hydrotalcite-like layered double hydroxide and a cobalt-iron spinel phase were prepared by coprecipitation from a solution of a mixture of magnesium, aluminum, cobalt(II), and iron(III) salts followed by hydrothermal treatment. The iron and cobalt contents in the samples were varied within a broad range. The thermal transformations of the prepared composites were examined by high-temperature X-ray diffraction, and the layered hydroxide phase was found to remain when heated up to 300°C. The specific magnetization and magnetic susceptibility of the materials were determined using a vibrating sample magnetometer; a rise in the iron and cobalt contents was found to increase the magnetization up to a certain limit. The obtained samples can be used as magnetic sorbents. The sorption capacity of materials was estimated using Congo red anionic dye as an example.

Keywords: magnetic materials, layered double hydroxides, iron, cobalt, Congo red, sorption

DOI: 10.1134/S096554412103004X

Layered double hydroxides (LDHs) are a class of natural and synthetic materials with a specific structure. Layers in hydrotalcite-like LDHs are similar to $Mg(OH)_2$ brucite and are hexagonally packed. In turn, brucite-like layers consist of octahedral unit cells with doubly or triply charged cations located in the center and surrounded by six hydroxide groups [1, 2].

The chemical composition of hydrotalcite-like LDHs is described by the general formula:

$$[M^{2+}_{1-x}M^{3+}_{x}(OH)_2]^{x+}(A^{n-})_{x/n} \cdot zH_2O,$$

where M^{2+} and M^{3+} are the brucite-like layer's cations, and A^{n-} designates the interlayer space's anions.

This class of compounds is notable because of their comparative lightness and the broad variation range of both the cationic and anionic compositions, which stimulates the formation of samples possessing catalytic [3–5], magnetic [6], electrical [7], and other properties [8].

The sorption and ion-exchange properties of LDHs are of particular interest [9–11], which is explained by their anion selectivity. Natural hydrotalcite-like materials are the only type of minerals that possess anion-exchange properties. Some researchers suggest utilizing synthetic LDHs for sorption treatment of water and air [12, 13].

Recently, sorbents possessing magnetic properties have attracted increasing attention [14, 15]. Magnetic separation is an exceptionally convenient method for separating powdered sorbents from a solution. Magnetic sorbents are usually represented by composite materials, one component of which, often an iron compound, possesses magnetic properties. Earlier we attempted to synthesize magnetic tetrametallic MgCo/AlFe LDHs. The prepared samples proved to have magnetic properties at room temperature and be able to act as effective sorbents to remove anionic dyes from solutions [16]. The phase composition of the samples showed that their magnetism results from the presence of a spinel-structured ($CoFe_2O_4$) impurity phase [17], i.e., that the synthesis produces composite materials.

This study focuses on the examination of the thermal stability and magnetic characteristics of tetrametallic-LDH-based sorbents and on the optimization of their composition.

EXPERIMENTAL

A series of hydrotalcite-like materials were synthesized by coprecipitation followed by hydrothermal treatment. The hydrotalcite-like materials simultaneously contained doubly charged magnesium and cobalt cations and triply

Table 1. Atomic proportions of metal cations in synthesized materials

Sample	Atomic proportions of cations[a]				M^{2+}/M^{3+}
	Mg^{2+}	Co^{2+}	Al^{3+}	Fe^{3+}	
MgCo10/AlFe10	0.672	0.091	0.203	0.035	3.22
MgCo20/AlFe20	0.595	0.168	0.186	0.051	3.21
MgCo30/AlFe30	0.524	0.225	0.172	0.079	2.97
MgCo40/AlFe40	0.447	0.306	0.139	0.109	3.04
MgCo50/AlFe50	0.366	0.382	0.126	0.127	2.97
MgCo5/AlFe30	0.670	0.054	0.167	0.110	2.61

[a] Calculated from energy-dispersive analysis.

charged aluminum and iron cations. The hydrotalcite-like materials also differed in the degree of substitution of cobalt and iron cations for magnesium and aluminum cations in the hydrotalcite structure, as well as in Co/Fe molar ratio. The metal cations were sourced from $Co(NO_3)_2 \cdot 6H_2O$, $Fe(NO_3)_3 \cdot 9H_2O$, $Mg(NO_3)_2 \cdot 6H_2O$, and $Al(NO_3)_3 \cdot 9H_2O$, the total concentration of which in the reaction mixture (a value specified for the synthesis) equaled 1 M for samples with Co/Fe = 1 : 1 and 0.5 M for Co/Fe = 1 : 2. In both cases, metal salt shots were dissolved in distilled water (molar ratio $M^{2+}/M^{3+} = 3$), after which a NaOH solution was added to the salt solution under constant stirring until pH 9–10. The resulting suspension was hydrothermally treated in an Autoclave Engineers Parker autoclave. Varying hydrothermal treatment conditions were imposed. Suspensions having Co/Fe = 1 : 1 (a molar ratio specified for the synthesis) were held at 140°C and 2.6 atm for 48 h. A sample with Co/Fe = 1 : 2 (hereinafter referred to as the optimized sample) was hydrothermally treated at 140°C and 1.6 atm for 6 h. On expiration of the holding period, the reactor was cooled, the mother liquor was decanted, and the precipitate was washed with distilled water and dried in a desiccator at 110°C for 4 h.

The prepared samples are designated as MgCoX/AlFeY, where X and Y are the atomic proportion of cobalt and iron, respectively, in relation to the doubly and triply charged metal cations in the initial reaction mixture.

The phase composition of the synthesized materials and thermal destruction products was determined by XRD using a Rigaku SmartLab X-ray diffractometer (CuK_α radiation) in a 2θ range of 5° to 80° with a step of 0.02° and a scanning rate of 3 deg/min. Heating was carried out to a specified temperature at a heating rate of 10 deg/min, and isothermal holding was 30 min at a specified temperature.

The elemental composition of the synthesized materials was determined by energy-dispersive analysis using a QUANTA 200 3D FEI high-resolution scanning electron microscope equipped with an energy-dispersive chemistry analyzer at an operating voltage of 20 kV.

The magnetic properties of the materials were examined by a JDAW-2000B vibrating sample magnetometer (Changchun, China) in a magnetic field range of –20 000 to 20 000 Oe at room temperature.

Textural characteristics were determined by low-temperature nitrogen adsorption/desorption on a TriStar 3020 analyzer at liquid nitrogen temperature (77 K).

The sorption properties of the optimized sample were examined using a Congo red solution as a model dye system. To obtain the sorption kinetic curves of Congo red, a series of 0.05 g shots of the synthesized material were poured with 25 mL of the dye solution with an initial concentration of 0.075 mmol/L, and held for specified time intervals. The sorption equilibrium was examined by a static method. 25 mL of the dye solution of specified concentration was added to 0.05 g of the sample, thoroughly agitated, and held for 3 h. The residual dye concentration in the solutions was determined by spectrophotometry, the solution having previously been separated from the sorbent by centrifugation. The optical densities of the solutions were recorded at a wavelength of 500 nm on a SPECORD 210 Plus spectrophotometer. All the adsorption experiments were performed at 25±1°C.

RESULTS AND DISCUSSION

The XRD confirmed the predominance of hydrotalcite-structured layered double hydroxides, as well as the presence of a spinel-structured ($CoFe_2O_4$) phase, in the synthesized samples [17]. All the samples are attracted to a magnet as integral materials, with no separation into individual structural elements either in air-dry samples or in aqueous solutions. The elemental composition of the samples is presented in Table 1.

The application of LDH-based materials is often limited because they exist in a rather narrow temperature

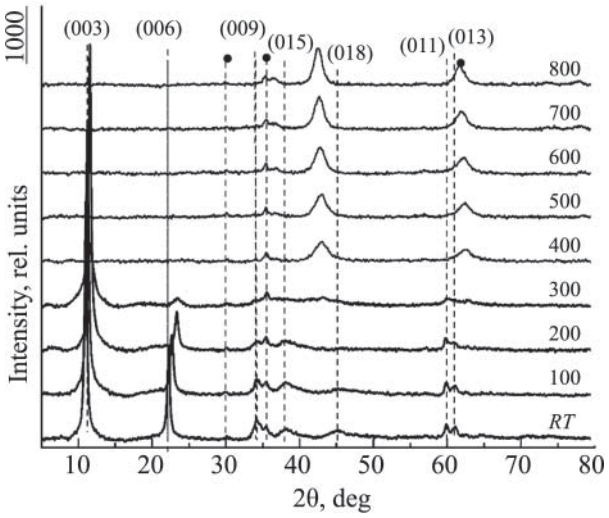

Fig. 1. Powder XRD patterns of MgCo10/AlFe10 during thermal treatment. Symbol (●) designates $CoFe_2O_4$.

range. In this regard, the investigation of their thermal transformations is of interest in its own right. According to available reports, during the thermal decomposition of layered double hydroxides their layered structure is retained within a broad temperature range. The thermal stability range of the layered structure depends on the initial LDH composition [18–20].

The thermal transformations of the samples were examined by high-temperature XRD. Figure 1 demonstrates typical powder XRD patterns obtained during the heating of MgCo10/AlFe10 as an example.

The XRD patterns clearly show the good retention of hydrotalcite structure at up to 200°C. Moreover, its marks are also observed after heating to 300°C, although only two low-intensity reflexes, corresponding to planes (003) and (006), remain in the XRD patterns.

Heating from 25 to 200°C predictably affects the positions of the reflexes corresponding to (003) and (006): they gradually shift towards high 2θ values, with a simultaneous intensity decline of reflex (006) with respect to (003) (Fig. 1). These changes are most likely caused by water removal from the interlayer space [19, 20]. The removal is accompanied by a decrease in the

Table 2. Crystal lattice parameters of the hydrotalcite phase after MgCo10/AlFe10 thermal treatment

Temperature, °C	*c*, Å	*a*, Å
25	23.88	3.09
100	23.46	3.09
200	22.84	3.09

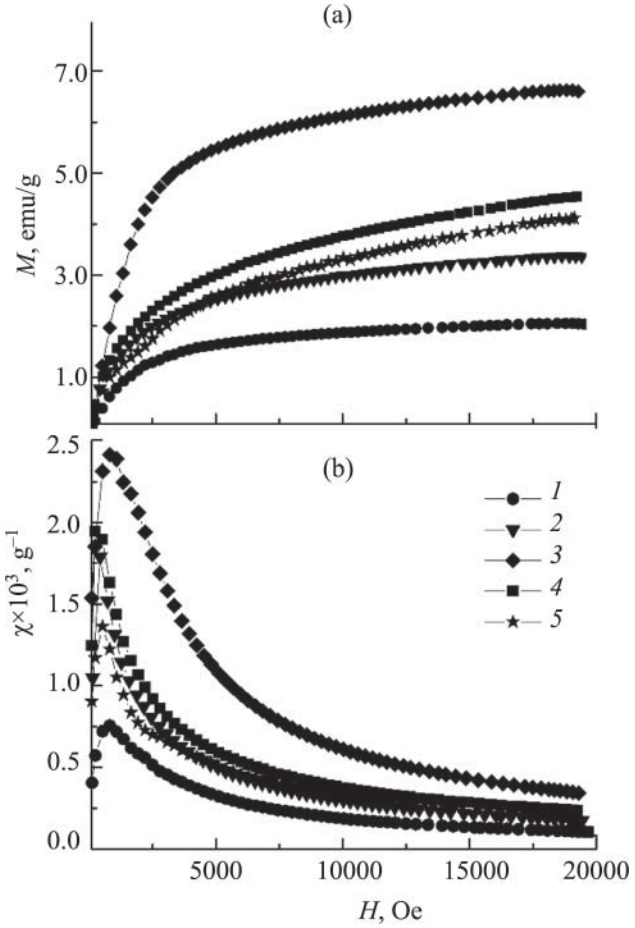

Fig. 2. (a) Specific magnetization vs. external field strength; and (b) specific magnetic susceptibility vs. external field strength: (*1*) MgCo10/AlFe10; (*2*) MgCo20/AlFe20; (*3*) MgCo30/AlFe30; (*4*) MgCo40/AlFe40; (*5*) MgCo50/AlFe50.

c value of the hexagonal crystal lattice and by a reduction of the interlayer distance (Table 2).

Further heating leads to the dehydroxylation of brucite-like layers and the removal of anions from the interlayer space, resulting in the formation of mixed oxide phases.

Notably, the spinel $CoFe_2O_4$ magnetic phase formed during the synthesis remains during heating within the entire assayed interval.

The magnetic properties of samples that differ in their cobalt and iron contents were examined by a vibration method. Figure 2a shows the curves of specific magnetization as a function of external field strength, and Fig. 2b shows the specific magnetic susceptibility as a function of external field strength. The curves are alike for all the samples.

It is known that all ferromagnetics are characterized by the presence of magnetic hysteresis. Figure 3 illustrates the hysteresis loop for the MgCo10/AlFe10 sample plotted at room temperature. The main magnetic parameters determined from the hysteresis loop are coercive force, residual magnetization, and maximum magnetization. For example, the MgCo10/AlFe10 sample achieves its maximum magnetization at 1.68 emu/g, with the residual magnetization and coercive force equal to 0.65 emu/g and 712 Oe, respectively.

It should be noted that the specific magnetization for the synthesized samples is significantly lower than that for the pure spinel $CoFe_2O_4$ phase (52.63 emu/g [21]). However, the maximum magnetization values achieved by our synthesized samples are sufficient for the successful removal of an LDH from the solutions. This allows them to be utilized as magnetic sorbents.

The data of Fig. 2 clearly show that the specific magnetic susceptibility and magnetization of the samples increase as their iron and cobalt contents rise, but this increase does not reach beyond a certain limit. The magnetic characteristics decline at high iron and cobalt contents. Presumably, this is associated with dimensional effects: spinel phase particles in the sample with maximum magnetism are about 20 to 25 nm, and their size grows with a rise in iron and cobalt contents. The size may influence the magnetic properties in accordance with a number of known mechanisms. Ferromagnetic nanoparticles are assumed to be single-domain, but their enlargement promotes their transition to multi-domain objects [22]. Another effect is attributed to the cluster state of magnetic particles: during the period of fine particles,

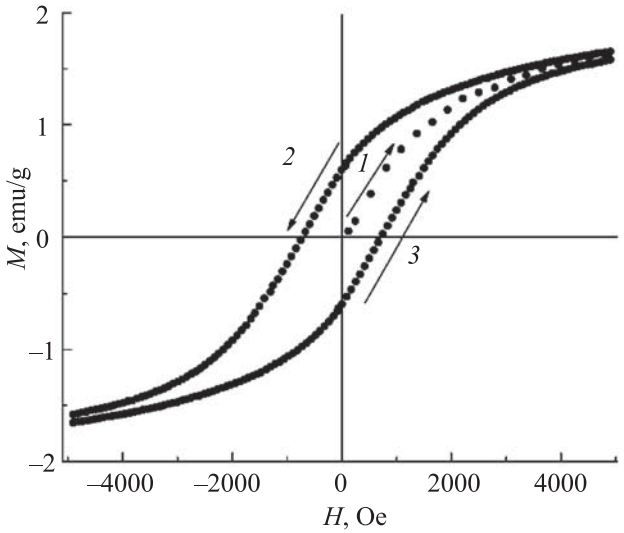

Fig. 3. Specific magnetization hysteresis for MgCo10/AlFe10: (*1*) initial magnetization curve; (*2*, *3*) curves of the main loop.

most of their atoms (or ions) are surface ones [22], which affects their magnetic properties. It is natural to assume that the growth in the magnetic phase content may be accompanied by its transition to the bulk state.

Consequently, there is no need to introduce high amounts of cobalt and iron to produce magnetic materials. Furthermore, as became evident when the magnetic phase's nature was identified, it is advisable to maintain the cobalt to iron ratio during the synthesis in the same stoichiometric proportion as they enter the magnetic spinel $CoFe_2O_4$. Finally, for practical reasons, it appeared rational to reduce the period of hydrothermal treatment of the sample and, if possible, to decrease the autoclave synthesis pressure. The optimization of the

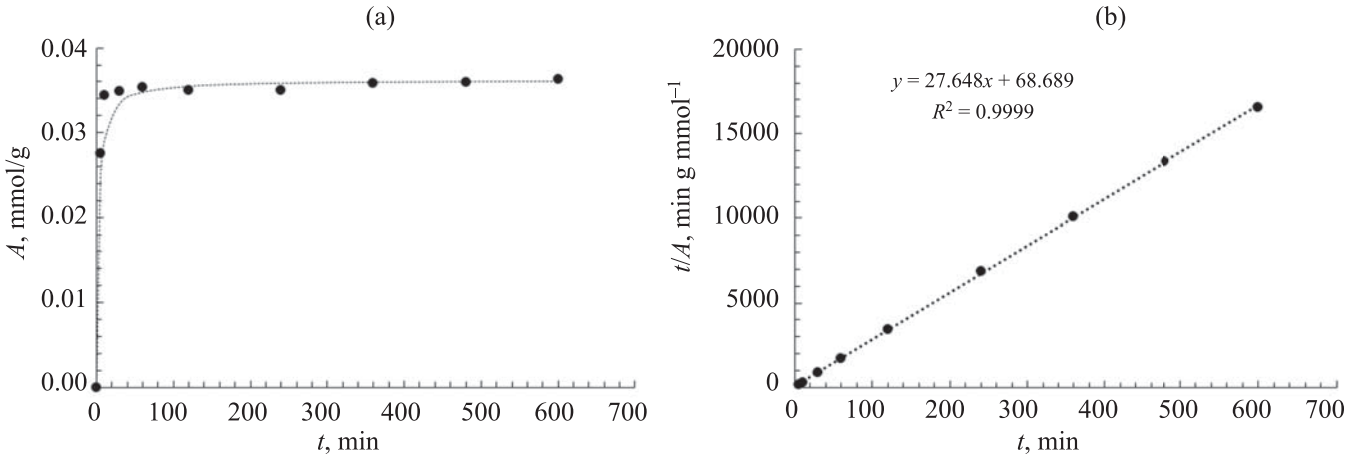

Fig. 4. (a) Sorption kinetic curve of Congo red dye for MgCo5/AlFe30; and (b) linearization of experimental data in the Ho and McKay's pseudo-second order model coordinates.

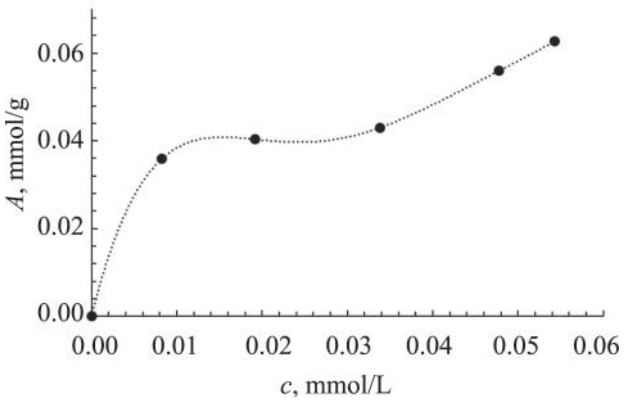

Fig. 5. Sorption isotherm of Congo red dye for MgCo5/AlFe30.

three abovementioned parameters resulted in the synthesis of the sample designated as MgCo5/AlFe30. Its chemical composition is presented in Table 1. The XRD pattern reflects the presence of a well-cristallized LDH and a cobalt-iron spinel phase. The sample has a specific surface of 21.4 m^2/g and a pore volume of 0.097 cm^3/g.

Figure 4a shows the sorption kinetic curve of Congo red for MgCo5/AlFe30. The presented data indicate that sorption equilibrium is reached within 60 min. This characterizes the sorbent as effective enough to remove the dye from an aqueous solution. The analysis of the experimental data showed that they are adequately described by Ho and McKay's pseudo-second order kinetic equation (Fig. 4b) [23].

Figure 5 presents the isotherm of Congo red sorption for MgCo5/AlFe30. Its shape can be attributed to the L3 type under the Giles classification [24]. The distinct inflexion at equilibrium concentrations above 0.02 mmol/L is probably explained by a change in the Congo red molecules' orientation from horizontal to vertical. Obviously, the sorption properties are determined by the LDH phase characteristics.

CONCLUSIONS

In summary, it was demonstrated that composite materials containing tetrametallic hydroxides and cobalt-iron spinel $CoFe_2O_4$ are readily formed by coprecipitation from a mixture of corresponding oxides followed by hydrothermal treatment. It was further shown that these materials retain their LDH structure when heated to at least 200°C, possess pronounced magnetic properties, and are able to rapidly adsorb Congo red anionic dye from aqueous solutions. It was found that a lower cobalt content during synthesis does not deteriorate the magnetic or sorption characteristics of the materials.

AUTHOR INFORMATION

O.V. Nestroinaya, ORCID: https://orcid.org/0000-0002-0868-094X

I.G. Ryl'tsova, ORCID: https://orcid.org/0000-0001-5248-5116

E.A. Tarasenko, ORCID: https://orcid.org/0000-0003-2094-1337

M.N. Yapryntsev, ORCID: https://orcid.org/0000-0001-8791-8102

A.A. Solov'eva, ORCID: https://orcid.org/0000-0001-5066-2932

O.E. Lebedeva, ORCID: https://orcid.org/0000-0002-5021-028X

FUNDING

The study described here was financially supported by a grant from the Russian Foundation for Basic Research (project no. 18-29-310011 mk). The study was carried out using scientific equipment of "Technologies and Materials" Center for Collective Use at the Belgorod State National Research University.

CONFLICT OF INTEREST

The authors declare no conflict of interest requiring disclosure in this article.

REFERENCES

1. Cavani, F., Trifirò, F., and Vaccari, A., *Catal. Today*, 1991, vol. 11, p. 173. https://doi.org/10.1016/0920-5861(91)80068-K
2. Tretyakov, Yu.D., Lukashin, A.V., and Eliseev, A.A., *Russ. Chem. Rev*., 2004, vol. 73, no. 9, p. 899. https://doi.org/10.1070/RC2004v073n09ABEH000918
3. Kuljiraseth, J., Wangriya, A., Malones, J.M.C., Klysubun, W., and Jitkarnka, S., *Appl. Catal. B: Environmental*, 2019, vol. 243, p. 415. https://doi.org/10.1016/j.apcatb.2018.10.073
4. Kankan, B., Sanchai, K., Jiang, D., Hongrui, L., Tingting, Y., Guorong, C., and Liyi, S., *Appl. Catal. B: Environmental*, 2019, vol. 252, p. 86. https://doi.org/10.1016/j.apcatb.2019.04.007
5. Krylova, M.V., Kulikov, A.B., Knyazev, M.I., and Krylova, A.Yu., *Chem. Technol. Fuels and Oils*, 2008, vol. 44, p. 339. https://doi.org/10.1007/s10553-008-0064-8
6. Li, Q., Xing, L., Lu, X., Li, N., and Mingxiang, X., *Inorg. Chem. Commun*., 2015, vol. 52, p. 46. https://doi.org/10.1016/j.inoche.2014.12.014
7. Fan, G., Li, F., Evans, D.G., and Duan, X., *Chem. Soc.*

Rev., 2014, no. 43, p. 7040.
https://doi.org/10.1039/C4CS00160E
8. Rives, V., del Arco, M., and Martín, C., *J. Control. Release*, 2013, no. 169, p. 28.
https://doi.org/10.1016/j.jconrel.2013.03.034
9. Lei, C., Zhu, X., Zhu, B., Jiang, C., Le, Y., and Yu, J., *J. Hazardous Mater*., 2017, vol. 321, p. 801.
https://doi.org/10.1016/j.jhazmat.2016.09.070
10. Goh, K.-H., Lim, T.-T., and Dong, Z., *Water Res*., 2008, vol. 42, p. 1343.
https://doi.org/10.1016/j.watres.2007.10.043
11. Chuang, Y.H., Tzou, Y.M., Wang, M.K., Liu, C.H., and Chiang, P.N., *Ind. Eng. Chem. Res.*, 2008, vol. 47, p. 3813.
https://doi.org/10.1021/ie071508e
12. Kameda, T., Tsuchiya, Y., Yamazaki, T., and Yoshioka, T., *Solid State Sci*., 2009, vol. 11, p. 2060.
https://doi.org/10.1016/j.solidstatesciences.2009.09.008
13. Chaara, D., Pavlovic, I., Bruna, F., Ulibarri, M.A., Draoui, K., and Barriga, C., *Appl. Clay Sci*., 2010, vol. 50, p. 292.
https://doi.org/10.1016/j.clay.2010.08.002
14. Ivanets, A.I., Srivastava, V., Roshchina, M.Yu., Sillanpää, M., Prozorovich, V.G.,and Pankov, V.V., *Ceramics Int*., vol. 44, no. 8, p. 9097.
https://doi.org/10.1016/j.ceramint.2018.02.117
15. Li, W., Zhang, J., Zhu, W., Qin, P., Zhou, Q., Lu, M., Zhao, W., Zhang, S., and Cai, Z., *Talanta*, 2020, vol. 208, p. 120440.
https://doi.org/10.1016/j.talanta.2019.120440
16. Ryl'tsova, I., Tarasenko, E., Nestroinaya, O., and Lebedeva, O., *Sorbts. Khromatograf. Protses*., 2019, vol. 19, no. 3, p. 305.
https://doi.org/10.17308/sorpchrom.2019.19/747
17. Nestroinia, O.V., Ryl'tsova, I.G., Yapryntsev, M.N., and Lebedeva, O.E., *Inorg. Mater*., 2020, vol. 56, no. 7, p. 747.
https://doi.org/10.1134/S0020168520070109
18. Kanezaki, E., *Solid State Ionics*, 1998, vol. 106, nos. 3–4, p. 279.
https://doi.org/10.1016/S0167-2738(97)00494-3
19. Radha, A.V., Thomas, G.S., Kamath, P.V., Antonyraj, C.A., and Kannan, S., *Bull. Mater. Sci*., 2010, vol. 33, no. 3, p. 319.
https://doi.org/10.1007/s12034-010-0049-1
20. Vaysse, C., Guerlou-Demourgues, L., and Delmas, C., *Inorg. Chem*., 2002, vol. 41, no. 25, p. 6905.
https://doi.org/10.1021/ic025542r
21. Ortiz-Quiñonez, J.-L., Pal, U., and Villanueva, M., *ACS Omega*, 2018, vol. 3, no. 11, p. 14986.
https://doi.org/10.1021/acsomega.8b02229
22. Frolov, G.I., Bachina, O.I., Zav'yalova, M.M., and Ravochkin, S.I., *Tech. Phys*., 2008, vol. 53, p. 1059.
https://doi.org/10.1134/S1063784208080136
23. Ho, Y.S. and McKay, G., *Process Biochem*., 1999, vol. 34, p. 451.
https://doi.org/10.1016/S0032-9592(98)00112-5
24. Giles, C.H., MacEwan, T.H., Nakhwa, S.N., and Smith, D., *J. Chem. Soc*., 1960, p. 3973.
https://doi.org/10.1039/JR9600003973